LOOKING INSIDE MAN: MEDICAL IMAGING

Osipov LV[1,a], Dolgushin MB[2,b], Mikhaylov AI[2,b], Epel B[3,c], Rumyantsev KA[4,5,d], Turoverov KK[4,d], Verkhusha VV[5,d], Kulikova EYu[6] ✉

[1] IzoMed Ltd., Moscow, Russia

[2] Department of Positron Emission Tomography,
N. N. Blokhin Russian Cancer Research Center, Moscow, Russia

[3] Department of Radiation and Cellular Oncology,
University of Chicago, Chicago, USA

[4] Laboratory of the Structural Dynamics, Stability and Folding of Proteins,
Institute of Cytology of Russian Academy of Sciences, Saint-Petersburg, Russia

[5] Department of Anatomy and Structural Biology,
Albert Einstein College of Medicine, New York, USA

[6] Pirogov Russian National Research Medical University, Moscow, Russia

[a] ultrasound technologies; [b] tomographic technologies; [c] oximetry; [d] fluorescence imaging

The rapid progress of medical sciences has brought about novel effective medications, new techniques that make surgery less traumatic, artificial materials that serve to replace tissues and organs, and robotic prostheses. Still, treatment success is largely a question of timely and accurate diagnosis and proper patient monitoring. Here, various imaging techniques come in handy. Those are often thought of as tools for anatomy visualization, but in fact, they are often highly effective for the assessment of the functional state of organs and tissues. Imaging techniques are so diverse that it is impossible to cover them all in one review. Therefore, we have decided to touch upon the most common and interesting ones, such as ultrasound imaging, tomography, oximetry and fluorescence imaging.

Keywords: ultrasound imaging, computed tomography, magnetic resonance imaging, positron emission tomography, oximetry *in vivo*, fluorescence imaging *in vivo*

✉ **Correspondence should be addressed:** Elena Kulikova
ul. Ostrovityanova, d. 1, Moscow, Russia, 117997; elena.yu.kulikova@gmail.com

Received: 15.08.2016 **Accepted:** 20.08.2016

ЗАГЛЯНУТЬ В ЧЕЛОВЕКА: ВИЗУАЛИЗАЦИЯ В МЕДИЦИНЕ

Л. В. Осипов[1,a], М. Б. Долгушин[2,b], А. И. Михайлов[2,b], Б. Эпель[3,c], К. А. Румянцев[4,5,d], К. К. Туроверов[4,d], В. В. Верхуша[5,d], Е. Ю. Куликова[6] ✉

[1] ООО «ИзоМед», Москва

[2] Отделение позитронной эмиссионной томографии,
Российский онкологический научный центр имени Н. Н. Блохина, Москва

[3] Отделение радиологии и клеточной онкологии,
Университет Чикаго, Чикаго, США

[4] Лаборатория структурной динамики, стабильности и фолдинга белков,
Институт цитологии РАН, Санкт-Петербург

[5] Отдел анатомии и структурной биологии,
Колледж медицины имени Альберта Эйнштейна, Нью-Йорк, США

[6] Российский национальный исследовательский медицинский университет имени Н. И. Пирогова, Москва

[a] раздел по ультразвуковым технологиям; [b] раздел по томографическим технологиям; [c] раздел по оксиметрии; [d] раздел по флуоресцентной визуализации

Медицина развивается стремительно: разрабатываются новые более эффективные препараты, предлагаются все менее травматичные способы оперативных вмешательств, а для замещения тканей и органов используются искусственные материалы и управляемые протезы. Однако по-прежнему успех лечения во многом определяется своевременным и точным диагностированием заболевания, а также адекватным мониторингом эффективности терапии. Эти задачи решают с применением различных технологий визуализации. Многие ассоциируют их с представлением анатомических структур тела, но в действительности гораздо чаще они позволяют определить функциональное состояние тканей и органов. Разнообразие технологий визуализации велико, и описать их все в одной работе не представляется возможным, поэтому для настоящего обзора были выбраны наиболее распространенные и интересные из них: ультразвуковые и томографические технологии, прижизненная оксиметрия и флуоресцентная визуализация.

Ключевые слова: ультразвуковая визуализация, компьютерная томография, магнитно-резонансная томография, позитронно-эмиссионная томография, оксиметрия *in vivo*, флуоресцентная визуализация *in vivo*

✉ **Для корреспонденции:** Куликова Елена Юрьевна
117997, г. Москва, ул. Островитянова, д. 1; elena.yu.kulikova@gmail.com

Статья поступила: 15.08.2016 **Статья принята к печати:** 20.08.2016

Ultrasound imaging

Ultrasound imaging (USI) is one of the most popular medical imaging techniques. Among the basic operating modes of ultrasound scanners are a two-dimensional B-mode for obtaining grayscale images and various Doppler modes. The latter include a spectral Doppler for blood flow measurements and a two-dimensional color flow mapping that provides information on the hemodynamics in vessels and the heart. Tissue Doppler is used for monitoring moving heart structures (the left ventricle, in the first place). In certain areas of application, ultrasound imaging in B-mode may seem less informative, compared to other visualization techniques, but Doppler scans have a huge advantage here, as they allow obtaining information in real time.

The basic ultrasound modes are constantly evolving. For better visualization of malignant tumors and other blastomas, B-mode elastography is being gradually introduced into clinical practice. It maps tissue stiffness in the scanned area for further comparison. There are two approaches to stiffness evaluation. The first one is compression-based; a compressive force is applied to the scanned area (such as breasts or the prostate gland), and ultrasound images before and after compression are compared. The second technique makes use of shear waves generated after slight tissue compression or by a pushing acoustic pulse in a prescribed direction [1, 2]. Both approaches have their own advantages, and premium-class ultrasound machines support both of these modes.

A major drawback of Doppler techniques is that they are angle-dependent, which may cause artifacts and hinder interpretation of blood flow and cardiac motion images. To overcome this limitation, new methods are being actively developed. For example, a vector image of blood flow in the heart was successfully obtained using complex processing algorithms for Doppler scans of blood flow and left ventricular wall movements.

Non-Doppler imaging is also evolving, including a B-flow technique and speckle-tracking echocardiograpy. The former is used for blood flow visualization and detection of plaques in blood vessels, while the latter assists in analyzing the motion of heart tissues [1].

Transducers for ultrasound scanners

High image quality is extremely important in USI, especially when studying deep tissues or working with complicated cases. Surveys of European ultrasonographers have revealed that most of them are not satisfied with the image quality of their scanners [3]. Here, development of novel transducers for ultrasound scanners can be a solution.

Matrix arrays are becoming increasingly popular. Unlike conventional transducers that make use of a one-dimensional array of piezoelectric elements, whose number n varies from 64 to 256, matrix transducers have a two-dimensional array of *n* x *m* active elements. They allow for controlled focusing during transmission and continuous focusing during reception in both the scan plane and the one perpendicular to it, thus forming a narrow beam of transmitted pulses and condensed diagram for received echoes from all scanned depths and improving contrast resolution. High 3D scanning rate and a capability to produce 4D images (3D in real time) by generating several acoustic beams at a time are crucial for full matrix array transducers [1]. The resulting volumetric images can be further used by cardiologists, gynecologists, obstetricians and surgeons.

Another promising approach to transducer manufacturing makes use of monocrystal transducers in which piezoceramics is replaced with artificial crystals; they exhibit better performance and allow for deeper scanning and higher resolution.

Micro-electro-mechanical systems (MEMS) are a conceptually different basis for transducer manufacturing. For example, piezoelectric micromachined ultrasound transducers (pMUT) contain tiny matrix arrays of miniature elements and can be used for transesophageal echocardiography; microsized matrix arrays find their application in high-frequency catheter probes designed to obtain volumetric images of internal heart structures. Another method (Capacitive micro-fabricated ultrasound transducers, cMUT) makes use of capacitive elements with a flexible membrane that improve transducer sensitivity and resolution [4].

Transmit and receive units

A key requirement for modern ultrasound scanners is a wide bandwidth of transmit/receive frequencies that allows for short pulses and, subsequently, a higher resolution in B-mode and color Doppler modes. But as the frequency increases, the tissues attenuate the signal more and the imaging depth decreases. The problem could be solved by increasing pulse energy, but it is not safe. To overcome this limitation, “complex” signals can be used, such as encoded pulse sequences. They are long and allow for larger scan depth in case of high-frequency probes; owing to the compression algorithm, high resolution capacity is retained.

Multi-angle imaging is increasingly used in high-class scanning systems that repeatedly scan one particular area at changing beam angles. Then, the obtained images are summed up for better contrast resolution, more accurate tissue differentiation and clearer visualization of organ borders. Obviously, the frame rate does not benefit here and decreases by the number of projections used.

Adaptive modes and automated measurements

The variety of operating modes and settings available for ultrasound imaging is unsurpassed. Clinicians are looking forward to ultrasound machines that would be easy to operate, especially paramedics and general practitioners who use this imaging technique for bedside testing (the so-called point-of-care applications). Manufacturers offer different preset modes in which settings are selected automatically depending on a diagnostic task or a scanned organ. Ultrasound machines can automatically select continuous focusing in the reception mode and frequency depending on the scan depth, maintain the same level of mappable maximum echo intensity at various depths, evaluate some important diagnostic parameters and subsequently compute diagnostic indices, measure intima-media thickness, etc.

A good example of an adaptive mode that considerably improves image quality is automated evaluation of sound propagation speed in the scanned area used later for image formation. Unlike focusing in the reception mode, continuous focusing in the transmission mode is normally impossible. Synthetic aperture ultrasound is an advanced technique that allows for dynamic focusing at transmission and forms an image after the incoming data are postprocessed [1]. The synthetic aperture technique provides higher image resolution without reducing the frame rate.

Automated measurements and computations make the work of the ultrasonographer much easier and are already

employed in cardiology, angiology, obstetrics, urology and other medical fields. However, they demand exceptional image quality. Most often, high contrast resolution and distinct contours are a must for accurate measurements. For example, special radiofrequency techniques are used for fine measurements of arterial diameter changes to assess vascular elasticity and evaluate intima-media thickness, which is important in monitoring atherosclerosis progression.

Tomography

Discovered in 1895, X-radiation was long a basis for all radiology techniques and is still used for obtaining planar images in roentgenography, mammography and fluoroscopy. The next evolutionary step in the development of medical imaging was tomography, a method based on obtaining cross-sectional images of internal structures of the scanned object by simultaneous translation of the X-ray tube and the plate (detector). The image quality remained poor until Godfrey Hounsfield and Allan Cormack invented computed tomography in 1969–1971. A combination of computer technologies and the X-ray left the planar images far behind.

Computed tomography

Computed tomography (CT) is a noninvasive technique for cross-sectional imaging based on the measurement of X-ray attenuation in tissues of various densities and complex mathematical (computer) processing of the collected data. CT is currently the most common tomography technique for human body scanning.

The evolution of CT is connected with the increasing number of detectors and simultaneously captured projections, that makes the procedure faster and expands scanning area per rotation. Early scanners utilized a step-by-step principle with one rotation of the X-ray tube per slice and a single X-ray tube interacting with one (first generation scanners; processing time of 4 minutes per slice) or several (second generation scanners; processing time of 20 seconds per slice) detectors [1]. Then, helical computed tomography was introduced (HCT; third generation scanners): the tube and the detectors simultaneously completed one clockwise rotation per table increment making the scanning procedure shorter. Further increase in the number of detectors and superimposition of layers substantially reduces imaging time and improves quality of reconstructed images [5].

Fourth generation scanners (multislice spiral computed tomography (MSCT) have several rows of stationary detectors attached to a ring (gantry). The X-ray tube rotates at high speed (up to 0.33 seconds per rotation) sending out a modified-shape beam to the multiple detector rows (up to 320 detector rows can simultaneously capture multiple cross-sections). Widely used premium-class scanners have 64 or 128 rows of detectors, while standard scanners used in clinical routine have 16 to 32 detector rows. After manufacturers stopped the “who can install more detectors” race, they turned to improving the techniques for image reconstruction, which determined further MSCT evolution. Unlike SCT, MSCT is capable of generating isotropic images of submillimeter-thick sections (0.5 mm) and retaining their quality during the subsequent reconstruction in different planes and correction of density data. This inspired the development of virtual endoscopy techniques, such as virtual colonography and bronchoscopy, that provide for highly accurate endoscopic images and can be used to perform virtual intravascular endoscopy, given that improved data postprocessing techniques are available [6].

Owing to higher scan rates, we can now assess the accumulation dynamics of radiographic contrast agents using higher spatial resolution. CT-angiography is almost in no way inferior to a direct angiographic examination, but in contrast to it, is noninvasive. Today, it is not only a routine technique for the evaluation of various blood flow defects (stenosis, aneurisms, total occlusions), but also a tool for the detection of vessel wall abnormalities (atherosclerotic plaques) where direct angiography is not an option. Using modern reconstruction techniques, we can obtain high-quality images at low absorbed radiation doses [7].

CT-perfusion makes use of tissue density measurements after intravenous administration of a radiographic contrast agent. The incoming data are mathematically processed and a number of blood flow parameters are calculated, the major being velocity, volume and time. Several methods can be applied to analyze a time-dependent profile of contrast agent concentration and evaluate tissue hemodynamics. A variety of obtained hemodynamic characteristics serve to differentiate between benign and malignant tumors, detect iatrogenic changes, grade tumor malignancy and estimate the extent of organ damage in patients with blood circulation disorders [8].

Of particular interest is dual energy CT that employs two X-ray sources, as its name implies. For heart scans (the heart is an object in motion), acquisition time is very short and must be synchronized with the cardiac rhythm. In MSCT, the minimal time required to collect all data from a non-moving slice (tube rotation time of 0.33 seconds) is 173 seconds, which means that tube half-turn provides for a sufficient temporal resolution in patients with normal heart beat (65-80 beats per second). However, patients with cardiac pathology often have elevated heart rates and are arrhythmic. Two X-ray tubes positioned at a 90° angle ensure a 83-second temporal resolution, which is a quarter of the tube full turn. Thus, obtaining high-quality images of the heart becomes possible even in patients with elevated heart rates [9].

Dual energy scanners have another important advantage: each tube can switch between different voltages and currents. Coupled with complex computations, such design ensures a better differentiation between tissues with similar densities, reduces the number of artifacts caused by nearby objects of various densities (improves quality of angiographic images and visualization of vascular flow and neoplasms located close to bones or metal implants), and allows for contrast enhancement quantification without native imaging. Tissues absorb radiation differently in the presence of iodinated contrast agents, which explains the effects listed above, while absorption properties of hydroxyapatites (a bone mineral) and metals do not change [10].

There are methods of computer data processing that can determine content of various salts in the scanned area by measuring changes in its absorption properties at different energy levels. They have already found their application in clinical routine, e.g., in the diagnosis of gout based on determining monosodium urate depositions [11].

Magnetic resonance imaging

Magnetic resonance imaging (MRI) is s a technique that uses the phenomenon of nuclear magnetic resonance for visualization of internal organs and tissues. The method is based on measuring the atomic nuclei electromagnetic response (hydrogen nuclei in most cases) excited by various

combinations of electromagnetic waves in a static magnetic field (0.5–3.0 Tesla) [12, 13].

MRI was initially used for brain scans (it is still the "gold standard" in neuroimaging) and was later employed to visualize other body regions. Advances in virtual coil emulation methods that use individual elements of surface coils allowed for automatic expansion of scanning areas to larger anatomic regions, including the whole body. In case of a whole-body MRI, a moving table and built-in receiver coils makes manual repositioning of the patient unnecessary [13].

Unlike CT, MRI does not expose patients to ionizing radiation and provides higher resolution for soft tissue scans, one of the reasons being its ability to suppress a signal from some tissue types. Organ-specific magnetic resonance contrast agents (gadoxetic acid for liver scans or superparamagnetic iron oxide nanoparticles for lymph node imaging) make MRI a "molecular"-oriented imaging technique, just like positron emission tomography (PET) [12, 13].

Diffusion-weighted imaging (DWI) is a form of MRI based on recording mobility (the area a particle covers per unit time) of protons labeled with radiofrequency pulses. This method allows for a semiquantitative evaluation of random Brownian motion (temperature-dependent migration) of water molecules in the body. Using DWI, we can assess the integrity of cell membranes and the intercellular matrix. DWI has found its application in the diagnosis of acute cerebral ischemias, such as acute and peracute stroke, where a CT scan is not an option. DWI is extensively used for the differential diagnosis of brain tumors and demyelinating diseases; whole-body DWI is a highly effective and sensitive method of cancer staging and a good screening technique for individuals at high risk for cancer or its relapse (combined with PET-CT, DWI reduces the radiation dose a patient is exposed to) [14].

DWI has also found its application in tractography. By measuring diffusion tensor, we can calculate its direction; then, upon collecting data on the geometric structure of tissues, we can understand in which direction large bundles of nerve and muscle fibers run. This information is valuable if a surgical treatment of brain and spinal cord tumors is planned or possible neurological risks must be assessed [15].

Magnetic resonance spectroscopy (MRS) is a technique that provides information on tissue biochemistry by measuring concentrations of different metabolites. For MRS, any nucleus with an odd atomic number can be used, though the best signal is generated by hydrogen nuclei. The technique was first suggested in the 1970s, but its evolution was long inhibited by the lack of adequate equipment [16]. Since MRS has strict requirements for field heterogeneity and is highly sensitive to organ motion, it is mostly used for brain and prostate gland scans. It is known that metabolic imbalances in tissues occur prior to clinical manifestations of the disease; because of that, MRS data can assist in the early diagnosis [17]. Owing to improved data processing algorithms, it is now possible to convert standard spectroscopy data to metabolic maps of large brain regions [18].

Magnetic resonance angiography (MRA) is used to visualize blood vessels anatomy and assess functional specifics of blood circulation. This technique is based on differentiating between signals from moving blood protons and static surrounding tissues. MRA allows obtaining vessel images without administering contrast agents to the patient [19].

A relatively new technique for the assessment of hemodynamics and perfusion of brain matter is perfusion MRI. It is more beneficial than CT-perfusion as it does not use X-radiation and does not need contrast agents for enhanced images, which is very important when performing scans on children [8, 20].

Functional MRI (fMRI) is a technique for mapping cortical activity of the brain; it can be used to examine individual anatomy/features of a patient's brain and image regions responsible for motion, vision, speech, memory and other high cortical functions. This technique registers increased blood flow in activated cortex areas [21].

Imaging capacities of modern MR scanners have offered a perfect solution to the problem of brain anatomy visualization (including blood and cerebrospinal fluid flow) and to some extent now assist in the assessment of brain functional state.

Positron emission tomography

PET was first introduced into clinical practice more than 30 years ago and was primarily used in neurology and cardiology. Since the 2000s, it has been in increasing demand in oncology: over 90 % of all PET scans are performed on cancer patients [22].

The physical principle behind this technique is registration of emission from a radiopharmaceutical (RF) accumulated in tissues. Healthy and pathologic tissues accumulate RFs differently depending (though not exclusively) on their functional state. The most common RF is ^{18}F-fluorodeoxyglucose (^{18}F-FDG) [22]. A combination of radionuclide technologies and tomography (PET-CT, PET-MRI) improves spatial visualization of anatomic structures and yields a wealth of information on tumor metabolism, thus solving a number of medical tasks. Those include early detection of disease progression or the spread of neoplasms, assessment of tumor response to treatment, differentiation between malignant and benign tumors and non-neoplastic lesions [23]. Figure 1 shows contribution of various imaging methods to the diagnosis of non-Hodgkin lymphoma [24].

^{18}F-FDG PET has proved to be highly effective in the diagnosis of lung, esophageal and colorectal cancers, head and neck tumors. An ^{18}F-FDG PET-CT scan is a "gold standard" in the diagnosis of melanoma and lymphomas and in screening for occult primary lesions in patients with metastatic cancer. Ordering an ^{18}F-FDG PET scan for patients with well-differentiated breast cancer (BC), thyroid, pancreatic, ovarian or testicular cancers and sarcomas is disputable [20]. In case of kidney, prostate or bladder cancer, hepatocellular carcinomas and neuroendocrine or brain tumors, ^{18}F-FDG PET is not quite informative, which can be compensated for by using other RFs. We are providing some examples below.

In case of brain tumors, the most commonly used radiotracers are those with negligible accumulation in the intact brain matter that reflect amino acid metabolism. The most popular RF is ^{11}C-methionine; it exhibits an almost 90% specificity in the diagnosis of intracranial tumors. ^{18}F-fluoroethyl-tyrosine is a next-generation radiotracer with a longer half-life; therefore, it can be used for a wider range of tasks. ^{18}F-thymidine reflects the dynamics of DNA assembly and helps to assess cell proliferation in tumors treated with anticancer drugs. A very interesting formulation is ^{11}C-sodium butyrate, a fatty amino acid with unique properties that allows for the assessment of both tumor hemodynamics (the extent of vascularization) and its metabolism [25]. Choline-containing agents labeled with ^{11}C or ^{18}F provide information on the formation of membrane complexes (phospholipids) and acetylcholine receptors. It is known that fast renewal and formation of cell membranes are typical for rapidly growing malignant tumors, and the pattern of RF accumulation can reflect this process [26].

When ordered for patients with breast cancer, PET does not play a role of the initial diagnostic procedure, but is used to assess biological activity of the initial neoplasm, detect regional and distant metastases and local recurrences and estimate treatment efficacy; for these purposes, PET is normally enhanced with ^{18}F-FDG [27]. However, some BC types are better detected with ^{18}F-fluoroestradiol that has affinity to estrogen receptors. Another RF, ^{18}F-Galacto-RGD, helps to visualize invasive ductal carcinomas and is used when a planned treatment includes angiogenesis inhibitors [28].

As a prostate cancer diagnostic tool, ^{18}F-FDG PET-CT exhibits limited efficacy, because ^{18}F-FDG is accumulated in the benign hyperplastic tissue of the gland. ^{18}F-choline and ^{11}C-choline that have become quite popular over the past few years are used instead. A PET-CT scan enhanced with choline-containing agents serves to detect cancer recurrences after radiation therapy, brachytherapy and prostatectomy (in case of a biochemical recurrence), as these treatments can seriously affect MRI results [29]. PET-CT is effective for verifying the diagnosis of regional prostate cancer and detecting metastases in regional lymph nodes. To detect distant metastases (bone metastases in particular), a number of examinations are normally carried out, including the whole body MRI, bone scintigraphy, liver ultrasound scanning and some others; conveniently, PET-CT can replace all of them [30]. Choline-containing radiotracers are not the only RFs assisting in prostate cancer diagnosing. Another novel PET tracer is ^{18}F-fluoro-dihydrotestosterone (FDHT). ^{18}F-FDHT PET rely on the increased expression of androgen receptors typical for both cancer and normal cells of the prostate gland [31]; therefore, it would be a better option to use FDHT for treatment monitoring but not for diagnosing primary prostate cancer. ^{68}Ga-PSMA is a radiotracer derived from a prostate-specific membrane antigen. It is highly specific and can be used if treatment with radioactive Y-90- or Lu-177-PSMA is planned [32].

Sensitivity of ^{18}F-FDG PET is too low to diagnose neuroendocrine tumors of various localization. Here, other RFs are employed: ^{18}F-luoro-L-dihydroxyphenylalanine, ^{11}C-hydroxy-L-tryptophan and somatostatin receptor ligands labeled with ^{68}Ga (^{68}Ga-DOTA-TOC, ^{68}Ga-DOTA-NOC, ^{68}Ga-DOTA-TATE) [33]. Comparative efficacy studies of scintigraphy and PET enhanced with similar peptides demonstrate high sensitivity and specificity of the latter, while a combination of PET and CT makes the procedure more informative [34].

If there is a suspicion of bone metastases, ^{18}F-NaF (sodium fluoride) can be used for PET-CT instead of ^{18}F-FDG. Its diagnostic value is similar to that of 99mTc-exametazime used for SPECT. A significant advantage of ^{18}F-NaF-PET-CT over bone scintigraphy is a lower radiation dose and higher spatial resolution, makes it possible to detect even the smallest metastases in the bones [35].

EPR oximetry in spectroscopy mode *in vivo*

Electron paramagnetic resonance (EPR) imaging is a rapidly evolving technique for visualization of spatial distribution of paramagnetic centers (PCs), molecules with unpaired electrons, spin labels and spin probes (SPs), and exploration of their kinetic properties, spectral parameters and relaxivity. EPR imaging is similar to magnetic resonance imaging; however, it has its own unique features [36]. For example, EPR imaging makes use of a 658 times weaker magnetic field, which eliminates the need for expensive superconducting magnets. Spatial distribution of PCs is detected using a linear magnetic field gradient G superimposed on the static magnetic field B_0. An additional magnetic field applied to PCs allows encoding their position.

High concentrations of PCs are rarely found in nature; therefore, EPR imaging employs various spin probes to obtain images. Depending on the problem PCs are synthesized for, they can be sensitive to various chemical and physical factors: viscosity, temperature, pH, redox potential and pO_2 partial pressure. PCs are administered intravenously or intra-arterially; in some cases, such as in monitoring malignant tumors, they are injected straight into the area of interest. Probes easily enter the intercellular volume and are cleared from the body in 10–50 minutes [37].

Oximetry is a major application area for modern EPR imaging. Molecular oxygen is essential for maintaining cellular balance. To function normally, tissues need adequate oxygen supply. Based on O_2 levels, a wide variety of conditions can be diagnosed. When dealing with cancers, it is important to know spatial distribution of oxygen in the tumor, because pO_2 levels

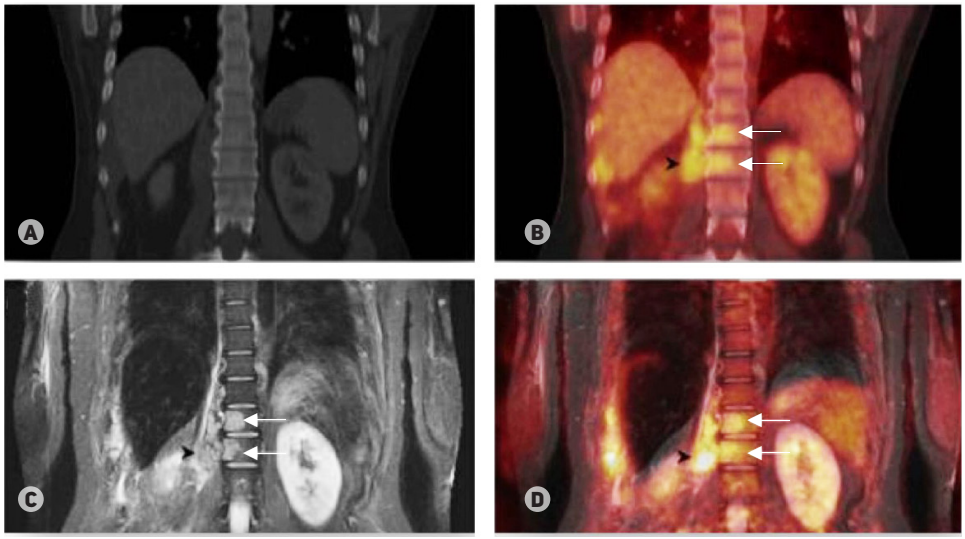

Fig. 1. Non-Hodgkin lymphoma spread to the bone marrow. Computed tomography in the bone window **(A)** detects paravertebral tumor masses, but does not see lesion-infiltrated vertebrae, while magnetic resonance imaging (C) can detect these lesions (shown by arrows) confirmed by hybrid technologies: PET-CT **(B)** and ^{18}F-fluorodeoxyglucose-enhanced PET-MRI **(D)**. Thus, MRI is more sensitive in the diagnosis of bone marrow lesions and detects the first signs of bone destruction and plasma cell infiltrates before osteoclast hyperstimulation can be observed (Buchender et al. [24])

largely determine tumor sensitivity to radiation or chemotherapy [38, 39]. Development of more accurate methods for pO_2 visualization in tissues can greatly widen the range of the targeted treatment applications in biology and medicine [40].

Recent advances in EPR oxymetry are linked to the use of triarylmethyl radicals as spin probes with narrow EPR lines, which contributes to the improvement of the image spatial resolution (0.5–1.0 mm) [41]. The SP rates of longitudinal (spin-lattice) and transverse relaxation are linearly dependent on pO_2 and allow detecting pO_2 levels with a 1 mmHg precision. The major drawback of this technique is that it requires SPs that have not yet been approved for clinical use.

To demonstrate practical application of EPR oximetry, we are providing the results of a study by Epel et al. [42] below. It was a preclinical study of oxygen-guided spatially modulated radiation therapy of tumors. The experiment was carried out on mice with a grown fibrosarcoma. The idea behind the study was as follows: lethal radiation dose for well-oxygenated malignant tissues is 3 times lower than for tissues with < 10 mmHg pO_2, therefore radiation dosage for different tumor regions can be varied. The radiation plan was delivered in two steps. First, 30 % tumor control dose (TCD_{30}) was delivered to the whole tumor. This dose is sufficient to kill well-oxygenated tumor cells with 99 % probability. Then, an additional dose boost was delivered to hypoxic tumor regions resistant to radiation. The cumulative radiation dose for these regions was comparable to TCD98. The second step required submillimeter precision of radiation delivery. In this study, treatment was delivered using a novel animal radiation therapy system (XRAD225Cx micro-CT/radiation therapy delivery system) and a set of 5 beams projecting at different angles. The beams were shaped using tungsten-infused plastic blocks printed on a 3D printer. Figure 2 shows stages of their fabrication based on EPR imaging data. Beam calculations take only 30 minutes after EPR data have been obtained. Time between EPR measurements and radiation therapy onset is critical here, as tissue oxygenation levels can change. Preliminary studies have demonstrated high efficacy of this technique.

Last year, National Institutes of Health, USA, funded pioneer clinical trials in which EPR oximetry in spectroscopy mode was used to predict radiation treatment efficacy. The success of the project and the inspiring results of our work have paved the way for the introduction of this technique into clinical practice. An EPR imager is a simple device and can be easily integrated into standard irradiators for better cancer treatment.

Fluorescence imaging

Fluorescence imaging is a universal technique for the analysis of various biological systems, from single molecules to whole organisms. Over the past two decades, the use of GFP-like fluorescent proteins (FPs) has made it possible to image dynamic processes inside cells and subsequently advanced the development of novel microscopy techniques. Currently, researchers are focusing on the development of genetically encoded optical biomarkers with near-infrared (NIR) light absorption and emission spectra in the so called 650–900 nm “optical window” of living tissues, where light is no longer absorbed by the hemoglobin of red blood cells and skin melanin, and is not yet absorbed by water molecules. Such properties are important for noninvasive imaging of dynamic processes occurring in deep tissues of mammals. Novel fluorescent biomarkers can find their application in basic research in biology and medicine, since they can replace X-ray in certain cases. However, attempts to obtain GFP-like FPs that would satisfy the spectral requirements described above have so far been unsuccessful.

The use of bacterial phytochrome complexes with biliverdin (BV, a product of heme catabolism present in animal and human tissues) as fluorescent biomarkers has proved to be the solution. Over the last few years, a number of bacterial phytochrome-based NIR FPs have been obtained capable of permanent fluorescence, photoactivation or split-system formation [43–48].

Specifically, NIR FPs of the iRFP family allowed for the visualization of small tumors during early stages and investigation of their growth and metastasis in model organisms [43, 49]. iRFP713 was successfully used for monitoring tumors located in deep organs, such as liver, prostate gland, brain, and intraosseous tumors [50]. Fluorescence imaging combined with computed tomography was used to observe inflammatory breast cancer progression and formation of its metastases in lymph nodes [51] and to detect migration pathways of melanoma cells [50].

NIR FPs have a great potential as biomarkers for preclinical studies of anticancer drugs and for visualization of tumor regression and recurrence upon treatment [52].

The ability to image labeled cells across the whole body of an animal makes NIR FPs promising biomarkers for stem cell research. Labeling cardiac progenitor cells with iRFP713 protein allowed for the visualization of myocardial repair in ischemic mice [53]. The ability of transplanted iRFP713-labeled bone marrow cells to restore haematopoiesis in X-ray irradiated mice was also shown [54].

Zero cytotoxicity of iRFP proteins encourages their use for labeling of not only individual cell lines or organs, but the whole organisms. Recently, a line of transgenic mice has been obtained with high expression of iRFP713 protein in all tissues and organs, including brain, heart, lungs, liver, kidneys, spleen, pancreas, thymus, bone and adipose tissue [54]. iRFP713 expression in the primary culture of hippocampal and retinal neurons of mice helped to visualize neurons and characterize their metabolism [55].

NIR FPs ability to effectively bind endogenous BV in protozoa is instrumental in testing novel antiparasitic drugs ex vivo and *in vivo* during preclinical studies. iRFP713-expressing cells of several *Leishmania* species were successfully used for the selection of potentially effective antiparasitic drugs, and for a several week observation of infection progression in mice [56].

Spectrally different NIR FPs allow for simultaneous observations of several tissues and organs in model organisms. The use of a pair of biomarkers of the iRFP family (iRFP670 and iRFP720) in a living mouse allowed for the simultaneous visualization of two closely located tumors labeled with different biomarkers [43]. An example of such imaging technique is shown in fig. 3. Owing to mathematical algorithms for image processing incorporated into modern microscopes and bioimaging systems, up to 5 spectrally different NIR FPs can be used simultaneously [43].

Photoactivated NIR FPs (PAiRFPs) have an advantage of ensuring highly sensitive bioimaging against strong autofluorescence background in tissues. To obtain images with high contrast ratio, a differential method is applied: a background signal is subtracted by comparing object’s images before and after PAiRFP photoactivation in tissue cells. Since PAiRFPs can be photoactivated, they are also used for selective photolabeling and short-term observations of the dynamics of groups of cells *in vivo* [46].

To study protein-protein interaction in cell cultures and living organisms, a novel iSplit NIR-sensor was developed whose

fluorescence is induced by interaction of complementary components, which drives the assembly of functional NIR FPs. Despite the irreversibility of complementation, iSplit can reflect the dynamics of rare recurring protein interactions due to a relatively rapid degradation of assembled complexes [47]. The advantage of another NIR split-sensor of protein interaction, IFP PCA, is reversibility of complementation. Its use allowed for the exploration of the interaction of several pairs of proteins in yeast and animal cells [57]. However, IFP PCA brightness in animal cells is an order of magnitude lower than that of iSplit, which requires the addition or injection of an extra amount of BV.

CONCLUSION

The variety of medical imaging techniques is impressive. Moreover, one and the same technique can enjoy multiple applications. However, all of them are designed to image the functional state of tissues and organs in the first place, facilitating the choice of the best treatment or allowing for the assessment of its efficacy.

In ultrasound imaging, high image quality is crucial and is an evolution vector for modern ultrasound scanners. Volumetric images (3D and 4D) have not yet enjoyed their widest application in the clinical setting. Their efficacy has not been proved yet, there are certain limitations to their use in some branches of medical science; clinicians often fail to interpret their results, and many clinics just do not have the appropriate state-of-art equipment. However, some clinicians believe that future belongs to volumetric images [58]. Another trend in US technologies is an increasing use of portable point-of-care US-scanners [58].

CT is evolving in the direction of more effective techniques for image reconstruction. New radiopharmaceuticals for PET and MRI enhancement are regularly tested. We might expect a boom of PET-MRI studies in the nearest future: combined modalities were introduced just a few years ago following the development of novel probes in 2010. PET-MRI provides for a better examination accuracy and a lower radiation dose a patient is exposed to [59]. Integrated PET-MRI can yield interesting results in the assessment of brain functions when enhanced with a combination of different radiotracers and used with specialized MRI protocols [60].

Oximetry *in vivo* is used in various areas of medical research, but its potential is most likely to be fully realized in measuring oxygen levels in malignant tumors for elaborating the best radiation therapy plan. Its clinical efficacy is expected to be proved in the next few years.

Studies that employed bacterial phytochrome-based NIR FPs demonstrate a high potential of these optical biomarkers for noninvasive bioimaging *in vivo* and suggest they could be used in preclinical trials [57, 61, 62].

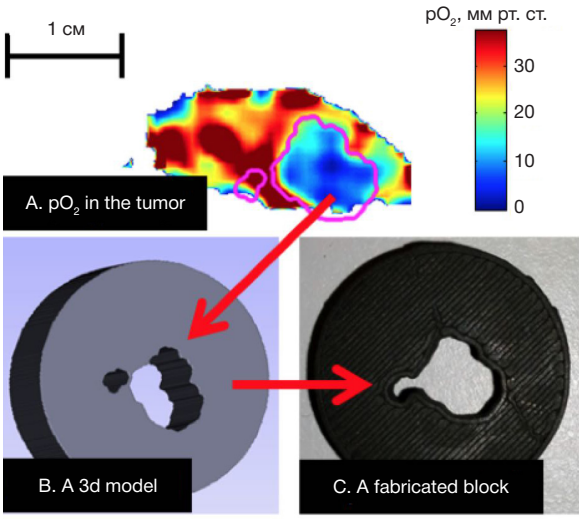

Fig. 2. Fabrication of blocks for targeted irradiation of a malignant tumor based on oxygen distribution in the tissue. **(A)** Slice of 3D image of pO_2 levels in different regions of mouse fibrosarcoma; a projection of tumor area selected for irradiation is outlined in magenta. **(B)** Computer model of the irradiation block. **(C)** Irradiation block printed on 3D printer (Epel et al. [42])

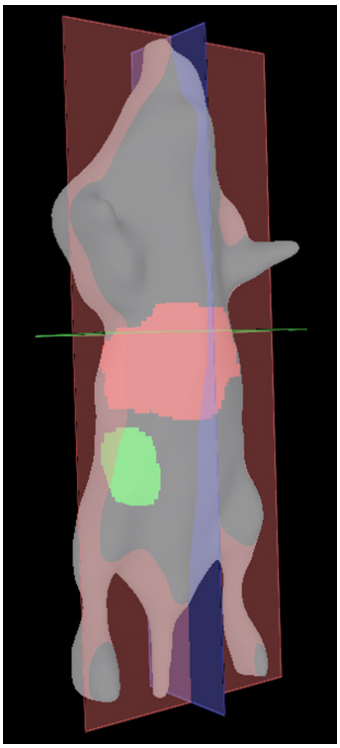

Fig. 3. Diffusion fluorescence image of a live mouse with a transplanted tumor and adenoviral infection in the liver. Tumor cells express iRFP670 protein, liver cells express iRFP713 protein. The liver and the tumor are shown in green and red pseudocolors, respectively (Scherbakova, Verkhusha, [43])

References

1. Osipov LV. Ul'trazvukovye diagnosticheskie pribory: rezhimy, metody i tekhnologii. Moscow: Izomed; 2011. 316 p. Russian.
2. Osipov LV. Tekhnologii elastografii v ul'trazvukovoy diagnostike. Obzor. Meditsinskiy alfavit: Diagnosticheskaya radiologiya i onkoterapiya. 2013; 3–4: 5–22. Russian.
3. Medimaging International staff writers. Poll's Findings Reveal Adaptable Imaging Systems to Transform Ultrasound Imaging. MedImaging.net. 2013 Sep 30.
4. Tai A. XDclear Transducer Technology [Internet]. GE Healthcare; c2016– [cited: 2016 Aug]. Available from: http://www3.gehealthcare.com/en.
5. Seeram E. Computed tomography: physical principles, clinical applications, and quality control. 4th ed. Saunders; 2015. 576 p.
6. Sun Z. Coronary Virtual Intravascular Endoscopy. In: Tintoiu IC, Underwood MJ, Cook SP, Kitabata H, Abbas A, editors. Coronary Graft Failure. Springer International Publishing; 2016. p. 555–70.
7. Schuhbaeck A, Achenbach S, Layritz C, Eisentopf J, Hecker F, Pflederer T, et al. Image quality of ultra-low radiation exposure

coronary CT angiography with an effective dose <0.1 mSv using high-pitch spiral acquisition and raw data-based iterative reconstruction. Eur Radiol. 2013; 23 (3): 597–606.
8. Bammer R. MR and CT Perfusion and Pharmacokinetic Imaging: Clinical Applications and Theory. Lippincott Williams and Wilkins; 2016. 1296 p.
9. Carrascosa PM, Garcia MJ, Cury RC, Leipsic JA. Dual-Energy CT. In: Carrascosa PM, Cury RC, Garcia MJ, Leipsic JA, editors. Dual-Energy CT in Cardiovascular Imaging. Springer International Publishing; 2015. p. 3–9.
10. Patino M, Prochowski A, Agrawal MD, Simeone FJ, Gupta R, Hahn PF, et al. Material Separation Using Dual-Energy CT: Current and Emerging Applications. Radiographics. 2016; 36 (4): 1087–105.
11. Fritz J, Henes JC, Fuld MK, Fishman EK, Horger MS. Dual-Energy Computed Tomography of the Knee, Ankle, and Foot: Noninvasive Diagnosis of Gout and Quantification of Monosodium Urate in Tendons and Ligaments. Semin Musculoskelet Radiol. 2016; 20 (1): 130–6.
12. Hashemi RH, Bradley WG, Lisanti CJ. MRI: The Basics. 3d ed. Lippincott Williams and Wilkins; 2012. 400 p.
13. Westbrook C, Roth CK, Talbot J. MRI in Practice. 4th ed. John Wiley and Sons; 2011. 456 p.
14. Taouli B, Beer AJ, Chenevert T, Collins D, Lehman C, Matos C, et al. Diffusion-weighted imaging outside the brain: Consensus statement from an ISMRM-sponsored workshop. J Magn Reson Imaging. 2016; 44 (3): 521–40.
15. Leote J, Nunes R, Cerqueira L, Ferreira HA. Corticospinal MRI tractography in space-occupying brain lesions by diffusion tensor and kurtosis imaging methods. EJNMMI phys. 2015; 2 (Suppl 1): A82.
16. Pinker K, Stadlbauer A, Bogner W, Gruber S, Helbich TH. Molecular imaging of cancer: MR spectroscopy and beyond. Eur J Radiol. 2012; 81 (3): 566–77.
17. Rosen Y, Lenkinski RE. Recent advances in magnetic resonance neurospectroscopy. Neurotherapeutics. 2007; 4 (3): 330–45.
18. Mabray MC, Barajas RF Jr, Cha S. Modern Brain Tumor Imaging. Brain Tumor Res Treat. 2015; 3 (1): 8–23.
19. Schulz J, Boyacioğlu R, Norris DG. Multiband multislab 3D time-of-flight magnetic resonance angiography for reduced acquisition time and improved sensitivity. Magn Reson Med. 2016; 75 (4): 1662–8.
20. Griffith B, Jain R. Perfusion imaging in neuro-oncology: basic techniques and clinical applications. Radiol Clin North Am. 2015; 53 (3): 497–511.
21. Uludağ K, Uğurbil K, Berliner L, editors. FMRI: From Nuclear Spins to Brain Functions. Springer US; 2015. 929 p.
22. Weissleder R. Molecular imaging in cancer. Science. 2006; 312 (5777): 1168–71.
23. Part 4: FDA-Approved PET/CT Tracers. In: Savir-Baruch B, Barron BJ. RadTool Nuclear Medicine Flash Facts. Springer International Publishing; 2016. 181–92.
24. Buchbender C, Heusner TA, Lauenstein TC, Bokisch A, Antoch G. Oncologic PET/MRI, part 2: bone tumors, soft-tissue tumors, melanoma, and lymphoma. J Nucl Med. 2012; 53 (8): 1244–52.
25. Tripathi RP. Recent trends in Molecular Imaging: PET/CT in Neurology. Ann Natl Acad Med Sci (India). 2014; 50 (1–2): 34–44.
26. Dolgushin MB, Odzharova AA, Tulin PE, Vikhrova NB, Nevzorov DI, Menkov MA, et al. [Use of ^{18}F-choline PET in Cerebral Gliomas]. Medical Visualization. 2014; 3: 73–83. Russian.
27. Lebron L, Greenspan D, Pandit-Taskar N. PET imaging of breast cancer: role in patient management. PET clin. 2015; Apr; 10 (2): 159–95.
28. Kurihara H, Shimizu C, Miyakita Y, Yoshida M, Hamada A, Kanayama Y, et al. Molecular imaging using PET for breast cancer. Breast Cancer. 2016; 23 (1): 24–32.
29. Mikhaylov AI, Tulin PE. Dvukhetapnaya PET/KT s 18F-ftorkholinom pri biokhimicheskikh retsidivakh raka predstatel'noy zhelezy. Evraziyskiy onkologicheskiy zhurnal. 2016; 2 (4): 388. Russian.
30. Dolgushin MB, Odzharova AA, Mikhailov AI, Shiryaev SV, Tulin PE, Nevzorov DI, et al. [Dual-stage ^{18}F-fluorocholine PET/CT scanning for biochemical recurrences of prostate cancer]. Cancer Urology.. 2015; 11 (2): 46–54. Russian.
31. Prosper A, Jadvar H. A Guided Tour of PET in Prostate Cancer. J Nucl Med. 2016; 57 (Suppl 2): 1319.
32. Barwick T. PET/CT imaging in prostate cancer. Cancer Imaging. 2015; 15 (Suppl 1): O15.
33. Ambrosini V, et al. PET/CT in Neuroendocrine Tumours. In: Ambrosini V, Fanti S, editors. PET/CT in Neuroendocrine Tumors. Springer International Publishing; 2016. p. 45–53.
34. Dolgushin MB, Shiryaev SV, Odzharova AA, Mikhaylov AI, Tulin PE, Nevzorov DI. PET-diagnostika v onkologii. Vestnik Moskovskogo onkologicheskogo obshchestva. 2015; 12 (603 Suppl): 63–74. Russian.
35. Jambor I, Kuisma A, Ramadan S, Huovinen R, Sandell M, Kajander S, et al. Prospective evaluation of planar bone scintigraphy, SPECT, SPECT/CT, 18F-NaF PET/CT and whole body 1.5 T MRI, including DWI, for the detection of bone metastases in high risk breast and prostate cancer patients: SKELETA clinical trial. Acta Oncol. 2016; 55 (1): 59–67.
36. Epel B, Halpern H. Electron paramagnetic resonance oxygen imaging in vivo. In: Gilbert BC, Murphy DM, Chechik V, editors. Electron Paramagnetic Resonance. Vol. 23. RSC Publishing; 2013. p. 180–208.
37. Matsumoto K, English S, Yoo J, Yamada K, Devasaharyam N, Cook JA, et al. Pharmacokinetics of a triarylmethyl-type paramagnetic spin probe used in EPR oximetry. Magnet Reson Med. 2004; 52 (4): 885–92.
38. Elas M, Bell R, Hleihel D, Barth ED, McFaul C, Haney CR, et al. Electron paramagnetic resonance oxygen image hypoxic fraction plus radiation dose strongly correlates with tumor cure in FSA fibrosarcomas. Int J Radiat Oncol Biol Phys. 2008; 71 (2): 542–9.
39. Elas M, Magwood JM, Butler B, Li C, Wardak R, Barth ED, et al. EPR Oxygen Images Predict Tumor Control by a 50 % Tumor Control Radiation Dose. Cancer Res. 2013; 73 (17): 5328–35.
40. Tatum JL, Kelloff GJ, Gillies RJ, Arbeit JM, Brown JM, Chao KS, et al. Hypoxia: Importance in tumor biology, noninvasive measurement by imaging, and value of its measurement in the management of cancer therapy. Int J Radiat Biol. 2006; 82 (10): 699–757.
41. Ardenkjaer-Larsen JH, Laursen I, Leunbach I, Ehnholm G, Wistrand LG, Petersson JS, et al. EPR and DNP properties of certain novel single electron contrast agents intended for oximetric imaging. J Magn Reson 1998; 133 (1): 1–12.
42. Epel B, Maggio C, Pelizzari C, Halpern HJ. Tumor oxygen-guided radiation therapy optimization. In: Oxygen Transport to Tissue XXXIX. Advances in Experimental Medicine and Biology. Springer. [In prep.].
43. Shcherbakova DM, Verkhusha VV. Near-infrared fluorescent proteins for multicolor in vivo imaging. Nat Methods. 2013; 10 (8): 751–4.
44. Shcherbakova DM, Baloban M, Pletnev S, Malashkevich VN, Xiao H, Dauter Z, et al. Molecular Basis of Spectral Diversity in Near-Infrared Phytochrome-Based Fluorescent Proteins. Chem Biol. 2015; 22 (11): 1540–51.
45. Rumyantsev KA, Shcherbakova DM, Zakharova NI, Emelyanov AV, Turoverov KK, Verkhusha VV. Minimal domain of bacterial phytochrome required for chromophore binding and fluorescence. Sci Rep. 2015; 5: 18348.
46. Piatkevich KD, Subach FV, Verkhusha VV. Far-red light photoactivatable near-infrared fluorescent proteins engineered from a bacterial phytochrome. Nat Commun. 2013; 4: 2153.
47. Filonov GS, Verkhusha VV. A near-infrared BiFC reporter for in vivo imaging of protein-protein interactions. Chem Biol. 2013; 20 (8): 1078–86.
48. Tchekanda E, Sivanesan D, Michnick SW. An infrared reporter to detect spatiotemporal dynamics of protein-protein interactions. Nat Methods. 2014; 11 (6): 641–4.
49. Lu Y, Darne CD, Tan IC, Wu G, Wilganowski N, Robinson H, et al. In vivo imaging of orthotopic prostate cancer with far-red gene reporter fluorescence tomography and in vivo and ex vivo validation. J Biomed Opt. 2013, 18 (10): 101305.
50. Jiguet-Jiglaire C, Cayol M, Mathieu S, Jeanneau C, Bouvier-Labit C, Ouafik L, et al. Noninvasive near-infrared fluorescent protein-based imaging of tumor progression and metastases in

deep organs and intraosseous tissues. J Biomed Opt. 2014, 19 (1): 16019.
51. Agollah GD, Wu G, Sevick-Muraca EM, Kwon S. In vivo lymphatic imaging of a human inflammatory breast cancer model. J Cancer. 2014; 5 (9): 774–83.
52. Condeelis J, Weissleder R. In vivo imaging in cancer. Cold Spring Harb Perspect Biol. 2010 Dec; 2 (12): a003848.
53. Wang Y, Zhou M, Wang X, Qin G, Weintraub NL, Tang Y. Assessing in vitro stem-cell function and tracking engraftment of stem cells in ischaemic hearts by using novel iRFP gene labelling. J Cell Mol Med. 2014; 18 (9): 1889–94.
54. Tran MT, Tanaka J, Hamada M, Sugiyama Y, Sakaguchi S, Nakamura M, et al. In vivo image analysis using iRFP transgenic mice. Exp Anim. 2014; 63 (3): 311–9.
55. Fyk-Kolodziej B, Hellmer CB, Ichinose T. Marking cells with infrared fluorescent proteins to preserve photoresponsiveness in the retina. Biotechniques. 2014;, 57 (5): 245–53.
56. Calvo-Alvarez, E.; Stamatakis, K.; Punzon, C.; Alvarez-Velilla, R.; Tejeria, A.; Escudero-Martinez, J. M.; Perez-Pertejo, Y.; Fresno, M.; Balana-Fouce, R.; Reguera, R. M. Infrared fluorescent imaging as a potent tool for in vitro, ex vivo and in vivo models of visceral leishmaniasis. PLoS Negl Trop Dis. 2015; 9 (3): e0003666.
57. Yao J, Kaberniuk AA, Li L, Shcherbakova DM, Zhang R, Wang L, et al. Multiscale photoacoustic tomography using reversibly switchable bacterial phytochrome as a near-infrared photochromic probe. Nat Methods. 2016, 13 (1): 67–73.
58. Zagoudis J, Fornell D. The Latest in Ultrasound Technology. Diagnostic and Interventional Cardiology [Internet]. 2016 Feb 12. Available from: http://www.dicardiology.com/article/latest-ultrasound-technology.
59. Kwon HW, Becker AK, Goo JM, Cheon GJ. FDG Whole-Body PET/MRI in Oncology: A Systematic Review. Nucl Med Mol Imaging. Epub 2016 Apr 7.
60. Vandenberghe S, Marsden PK. PET-MRI: a review of challenges and solutions in the development of integrated multimodality imaging. Phys Med Biol. 2015; 60 (4): R115–54.
61. Deliolanis NC, Ale A, Morscher S, Burton NC, Schaefer K, Radrich K, et al. Deep-tissue reporter-gene imaging with fluorescence and optoacoustic tomography: a performance overview. Mol Imaging Biol. 2014; 16 (5): 652–60.
62. Krumholz A, Shcherbakova DM, Xia J, Wang LV, Verkhusha VV. Multicontrast photoacoustic in vivo imaging using near-infrared fluorescent proteins. Sci Rep. 2014; 4: 3939.

Литература

1. Осипов Л. В. Ультразвуковые диагностические приборы: режимы, методы и технологии. М.: Изомед; 2011. 316 с.
2. Осипов Л. В. Технологии эластографии в ультразвуковой диагностике. Обзор. Медицинский алфавит: Диагностическая радиология и онкотерапия. 2013; 3–4: 5–22.
3. Medimaging International staff writers. Poll's Findings Reveal Adaptable Imaging Systems to Transform Ultrasound Imaging. MedImaging.net. 2013 Sep 30.
4. Tai A. XDclear Transducer Technology [Интернет]. GE Healthcare; c2016– [дата обращения: август 2016 г.]. Доступно по ссылке: http://www3.gehealthcare.com/en.
5. Seeram E. Computed tomography: physical principles, clinical applications, and quality control. 4th ed. Saunders; 2015. 576 p.
6. Sun Z. Coronary Virtual Intravascular Endoscopy. In: Tintoiu IC, Underwood MJ, Cook SP, Kitabata H, Abbas A, editors. Coronary Graft Failure. Springer International Publishing; 2016. p. 555–70.
7. Schuhbaeck A, Achenbach S, Layritz C, Eisentopf J, Hecker F, Pflederer T, et al. Image quality of ultra-low radiation exposure coronary CT angiography with an effective dose <0.1 mSv using high-pitch spiral acquisition and raw data-based iterative reconstruction. Eur Radiol. 2013; 23 (3): 597–606.
8. Bammer R. MR and CT Perfusion and Pharmacokinetic Imaging: Clinical Applications and Theory. Lippincott Williams and Wilkins; 2016. 1296 p.
9. Carrascosa PM, Garcia MJ, Cury RC, Leipsic JA. Dual-Energy CT. In: Carrascosa PM, Cury RC, Garcia MJ, Leipsic JA, editors. Dual-Energy CT in Cardiovascular Imaging. Springer International Publishing; 2015. p. 3–9.
10. Patino M, Prochowski A, Agrawal MD, Simeone FJ, Gupta R, Hahn PF, et al. Material Separation Using Dual-Energy CT: Current and Emerging Applications. Radiographics. 2016; 36 (4): 1087–105.
11. Fritz J, Henes JC, Fuld MK, Fishman EK, Horger MS. Dual-Energy Computed Tomography of the Knee, Ankle, and Foot: Noninvasive Diagnosis of Gout and Quantification of Monosodium Urate in Tendons and Ligaments. Semin Musculoskelet Radiol. 2016; 20 (1): 130–6.
12. Hashemi RH, Bradley WG, Lisanti CJ. MRI: The Basics. 3d ed. Lippincott Williams and Wilkins; 2012. 400 p.
13. Westbrook C, Roth CK, Talbot J. MRI in Practice. 4th ed. John Wiley and Sons; 2011. 456 p.
14. Taouli B, Beer AJ, Chenevert T, Collins D, Lehman C, Matos C, et al. Diffusion-weighted imaging outside the brain: Consensus statement from an ISMRM-sponsored workshop. J Magn Reson Imaging. 2016; 44 (3): 521–40.
15. Leote J, Nunes R, Cerqueira L, Ferreira HA. Corticospinal MRI tractography in space-occupying brain lesions by diffusion tensor and kurtosis imaging methods. EJNMMI phys. 2015; 2 (Suppl 1): A82.
16. Pinker K, Stadlbauer A, Bogner W, Gruber S, Helbich TH. Molecular imaging of cancer: MR spectroscopy and beyond. Eur J Radiol. 2012; 81 (3): 566–77.
17. Rosen Y, Lenkinski RE. Recent advances in magnetic resonance neurospectroscopy. Neurotherapeutics. 2007; 4 (3): 330–45.
18. Mabray MC, Barajas RF Jr, Cha S. Modern Brain Tumor Imaging. Brain Tumor Res Treat. 2015; 3 (1): 8–23.
19. Schulz J, Boyacioğlu R, Norris DG. Multiband multislab 3D time-of-flight magnetic resonance angiography for reduced acquisition time and improved sensitivity. Magn Reson Med. 2016; 75 (4): 1662–8.
20. Griffith B, Jain R. Perfusion imaging in neuro-oncology: basic techniques and clinical applications. Radiol Clin North Am. 2015; 53 (3): 497–511.
21. Uludağ K, Uğurbil K, Berliner L, editors. FMRI: From Nuclear Spins to Brain Functions. Springer US; 2015. 929 p.
22. Weissleder R. Molecular imaging in cancer. Science. 2006; 312 (5777): 1168–71.
23. Part 4: FDA-Approved PET/CT Tracers. In: Savir-Baruch B, Barron BJ. RadTool Nuclear Medicine Flash Facts. Springer International Publishing; 2016. 181–92.
24. Buchbender C, Heusner TA, Lauenstein TC, Bokisch A, Antoch G. Oncologic PET/MRI, part 2: bone tumors, soft-tissue tumors, melanoma, and lymphoma. J Nucl Med. 2012; 53 (8): 1244–52.
25. Tripathi RP. Recent trends in Molecular Imaging: PET/CT in Neurology. Ann Natl Acad Med Sci (India). 2014; 50 (1–2): 34–44.
26. Долгушин М. Б., Оджарова А. А., Тулин П. Е., Вихрова Н. Б., Невзоров Д. И., Меньков М. А. и др. ПЭТ с ^{18}F-фторхолином при исследовании глиальных опухолей головного мозга. Медицинская визуализация. 2014; 3: 73–83.
27. Lebron L, Greenspan D, Pandit-Taskar N. PET imaging of breast cancer: role in patient management. PET clin. 2015; Apr; 10 (2): 159–95.
28. Kurihara H, Shimizu C, Miyakita Y, Yoshida M, Hamada A, Kanayama Y, et al. Molecular imaging using PET for breast cancer. Breast Cancer. 2016; 23 (1): 24–32.
29. Михайлов А. И., Тулин П. Е. Двухэтапная ПЭТ/КТ с 18F-фторхолином при биохимических рецидивах рака предстательной железы. Евразийский онкологический журнал. 2016; 2 (4): 388.
30. Долгушин М. Б., Оджарова А. А., Михайлов А. И., Ширяев С. В., Тулин П. Е., Невзоров Д. И. и др. ПЭТ/КТ с ^{18}F-фторхо-

лином в режиме двухэтапного сканирования при биохимических рецидивах рака предстательной железы. Онкоурология. 2015; 11 (2): 46–54.
31. Prosper A, Jadvar H. A Guided Tour of PET in Prostate Cancer. J Nucl Med. 2016; 57 (Suppl 2): 1319.
32. Barwick T. PET/CT imaging in prostate cancer. Cancer Imaging. 2015; 15 (Suppl 1): O15.
33. Ambrosini V, et al. PET/CT in Neuroendocrine Tumours. In: Ambrosini V, Fanti S, editors. PET/CT in Neuroendocrine Tumors. Springer International Publishing; 2016. p. 45–53.
34. Долгушин М. Б., Ширяев С. В., Оджарова А. А., Тулин П. Е., Невзоров Д. И. ПЭТ-диагностика в онкологии. Вестник Московского онкологического общества. 2015; 12 (603 Приложение): 63–74.
35. Jambor I, Kuisma A, Ramadan S, Huovinen R, Sandell M, Kajander S, et al. Prospective evaluation of planar bone scintigraphy, SPECT, SPECT/CT, 18F-NaF PET/CT and whole body 1.5 T MRI, including DWI, for the detection of bone metastases in high risk breast and prostate cancer patients: SKELETA clinical trial. Acta Oncol. 2016; 55 (1): 59–67.
36. Epel B, Halpern H. Electron paramagnetic resonance oxygen imaging in vivo. In: Gilbert BC, Murphy DM, Chechik V, editors. Electron Paramagnetic Resonance. Vol. 23. RSC Publishing; 2013. p. 180–208.
37. Matsumoto K, English S, Yoo J, Yamada K, Devasaharyam N, Cook JA, et al. Pharmacokinetics of a triarylmethyl-type paramagnetic spin probe used in EPR oximetry. Magnet Reson Med. 2004; 52 (4): 885–92.
38. Elas M, Bell R, Hleihel D, Barth ED, McFaul C, Haney CR, et al. Electron paramagnetic resonance oxygen image hypoxic fraction plus radiation dose strongly correlates with tumor cure in FSA fibrosarcomas. Int J Radiat Oncol Biol Phys. 2008; 71 (2): 542–9.
39. Elas M, Magwood JM, Butler B, Li C, Wardak R, Barth ED, et al. EPR Oxygen Images Predict Tumor Control by a 50 % Tumor Control Radiation Dose. Cancer Res. 2013; 73 (17): 5328–35.
40. Tatum JL, Kelloff GJ, Gillies RJ, Arbeit JM, Brown JM, Chao KS, et al. Hypoxia: Importance in tumor biology, noninvasive measurement by imaging, and value of its measurement in the management of cancer therapy. Int J Radiat Biol. 2006; 82 (10): 699–757.
41. Ardenkjaer-Larsen JH, Laursen I, Leunbach I, Ehnholm G, Wistrand LG, Petersson JS, et al. EPR and DNP properties of certain novel single electron contrast agents intended for oximetric imaging. J Magn Reson 1998; 133 (1): 1–12.
42. Epel B, Maggio C, Pelizzari C, Halpern HJ. Tumor oxygen-guided radiation therapy optimization. In: Oxygen Transport to Tissue XXXIX. Advances in Experimental Medicine and Biology. Springer. [In prep.].
43. Shcherbakova DM, Verkhusha VV. Near-infrared fluorescent proteins for multicolor in vivo imaging. Nat Methods. 2013; 10 (8): 751–4.
44. Shcherbakova DM, Baloban M, Pletnev S, Malashkevich VN, Xiao H, Dauter Z, et al. Molecular Basis of Spectral Diversity in Near-Infrared Phytochrome-Based Fluorescent Proteins. Chem Biol. 2015; 22 (11): 1540–51.
45. Rumyantsev KA, Shcherbakova DM, Zakharova NI, Emelyanov AV, Turoverov KK, Verkhusha VV. Minimal domain of bacterial phytochrome required for chromophore binding and fluorescence. Sci Rep. 2015; 5: 18348.
46. Piatkevich KD, Subach FV, Verkhusha VV. Far-red light photoactivatable near-infrared fluorescent proteins engineered from a bacterial phytochrome. Nat Commun. 2013; 4: 2153.
47. Filonov GS, Verkhusha VV. A near-infrared BiFC reporter for in vivo imaging of protein-protein interactions. Chem Biol. 2013; 20 (8): 1078–86.
48. Tchekanda E, Sivanesan D, Michnick SW. An infrared reporter to detect spatiotemporal dynamics of protein-protein interactions. Nat Methods. 2014; 11 (6): 641–4.
49. Lu Y, Darne CD, Tan IC, Wu G, Wilganowski N, Robinson H, et al. In vivo imaging of orthotopic prostate cancer with far-red gene reporter fluorescence tomography and in vivo and ex vivo validation. J Biomed Opt. 2013, 18 (10): 101305.
50. Jiguet-Jiglaire C, Cayol M, Mathieu S, Jeanneau C, Bouvier-Labit C, Ouafik L, et al. Noninvasive near-infrared fluorescent protein-based imaging of tumor progression and metastases in deep organs and intraosseous tissues. J Biomed Opt. 2014, 19 (1): 16019.
51. Agollah GD, Wu G, Sevick-Muraca EM, Kwon S. In vivo lymphatic imaging of a human inflammatory breast cancer model. J Cancer. 2014; 5 (9): 774–83.
52. Condeelis J, Weissleder R. In vivo imaging in cancer. Cold Spring Harb Perspect Biol. 2010 Dec; 2 (12): a003848.
53. Wang Y, Zhou M, Wang X, Qin G, Weintraub NL, Tang Y. Assessing in vitro stem-cell function and tracking engraftment of stem cells in ischaemic hearts by using novel iRFP gene labelling. J Cell Mol Med. 2014; 18 (9): 1889–94.
54. Tran MT, Tanaka J, Hamada M, Sugiyama Y, Sakaguchi S, Nakamura M, et al. In vivo image analysis using iRFP transgenic mice. Exp Anim. 2014; 63 (3): 311–9.
55. Fyk-Kolodziej B, Hellmer CB, Ichinose T. Marking cells with infrared fluorescent proteins to preserve photoresponsiveness in the retina. Biotechniques. 2014;, 57 (5): 245–53.
56. Calvo-Alvarez, E.; Stamatakis, K.; Punzon, C.; Alvarez-Velilla, R.; Tejeria, A.; Escudero-Martinez, J. M.; Perez-Pertejo, Y.; Fresno, M.; Balana-Fouce, R.; Reguera, R. M. Infrared fluorescent imaging as a potent tool for in vitro, ex vivo and in vivo models of visceral leishmaniasis. PLoS Negl Trop Dis. 2015; 9 (3): e0003666.
57. Yao J, Kaberniuk AA, Li L, Shcherbakova DM, Zhang R, Wang L, et al. Multiscale photoacoustic tomography using reversibly switchable bacterial phytochrome as a near-infrared photochromic probe. Nat Methods. 2016, 13 (1): 67–73.
58. Zagoudis J, Fornell D. The Latest in Ultrasound Technology. Diagnostic and Interventional Cardiology [Интернет]. 12 февраля 2016 г. Доступно по ссылке: http://www.dicardiology.com/article/latest-ultrasound-technology.
59. Kwon HW, Becker AK, Goo JM, Cheon GJ. FDG Whole-Body PET/MRI in Oncology: A Systematic Review. Nucl Med Mol Imaging. Epub 2016 Apr 7.
60. Vandenberghe S, Marsden PK. PET-MRI: a review of challenges and solutions in the development of integrated multimodality imaging. Phys Med Biol. 2015; 60 (4): R115–54.
61. Deliolanis NC, Ale A, Morscher S, Burton NC, Schaefer K, Radrich K, et al. Deep-tissue reporter-gene imaging with fluorescence and optoacoustic tomography: a performance overview. Mol Imaging Biol. 2014; 16 (5): 652–60.
62. Krumholz A, Shcherbakova DM, Xia J, Wang LV, Verkhusha VV. Multicontrast photoacoustic in vivo imaging using near-infrared fluorescent proteins. Sci Rep. 2014; 4: 3939.